Astron. Astrophys. 354, 573–578 (2000)

ASTRONOMY AND ASTROPHYSICS

Shaping of elliptical planetary nebulae

The influence of dust-driven winds of AGB stars

Christian Reimers[1], **Ernst A. Dorfi**[1], **and Susanne Höfner**[2,1]

[1] Institute for Astronomy (IfA), University of Vienna, Türkenschanzstrasse 17, 1180 Vienna, Austria
[2] Uppsala Astronomical Observatory, Box 515, 75120 Uppsala, Sweden

Received 12 November 1999 / Accepted 2 December 1999

Abstract. We calculated a model to investigate the shaping of a PN morphological group, i.e. elliptical PNe, in terms of the so-called Interacting Winds Model. The angle-dependent mass loss generated by a dust driven wind due to a slow rotation of the AGB star is an effective way for the shaping of PNe. The matter which is more concentrated in the equatorial region of the star influences the flow of the fast hot wind originating from the central star, resulting in elliptical or weakly bipolar shapes for the corresponding PNe. A wide range of elliptical shapes can be explained by this model. In contrast to previous studies the angle-dependent mass loss on the AGB is not parameterized by an arbitrary formula but is taken from self-consistent dust-driven wind models. Furthermore we discuss the influence of the different inclination of the PNe in the sky, the interaction with an inhomogenous interstellar medium and the possible effect of a magnetic field in or around the old AGB star. Using detailed morphology studies with the Hubble Space Telescope (HST) we discuss possible scenarios to explain the sometimes very complex structures.

Key words: stars: AGB and post-AGB – ISM: planetary nebulae: general – ISM: planetary nebulae: individual: Abell 75 – ISM: planetary nebulae: individual: Abell 78 – ISM: planetary nebulae: individual: NGC 3132

1. Introduction

Stars on the asymptotic giant branch (AGB) are very extended objects with radii of the order of $10^{14}\,\mathrm{cm}$ (e.g. see Habing 1996). Due to magnetic braking during their lifetime and their large diameters the rotation rate will in general be small but some AGB stars may exhibit faster rotation rates like V Hya (Barnbaum et al. 1995) caused by angular momentum transfer from a binary and/or planetary system. However, from stability considerations the rotational velocities at the stellar photosphere cannot exceed a few $\mathrm{km\,s^{-1}}$.

During their evolution along the AGB these stars generate a massive dust driven wind and this mass loss deposits a large amount of stellar material in the surroundings. According to the models presented by Dorfi & Höfner (1996) the rotation of these AGB stars leading to a preferential mass loss with higher velocities in the equatorial plane. The angle-dependent mass loss rates obtained from this model are taken to investigate the influence on the shaping of planetary nebulae (PNe).

The accepted model to reproduce the shapes of the observed PNe is based on the Interacting Winds Model (hereafter IWM) by Kwok (1982) and Kahn (1982). In the IWM the the fast wind ($\sim 2000\,\mathrm{km\,s^{-1}}$) from the hot central star of the PN blows into the slow wind ($\sim 10\,\mathrm{km\,s^{-1}}$) produced during the preceding AGB phase. As a result of this interaction the inner region of the slow wind is compressed into a dense shell which will be illuminated by the energetic UV radiation of the central object so we can see the ring-like shape of the PN.

2. Interacting winds model (IWM)

2.1. AGB winds

During the late AGB-phase most of the initial stellar mass is lost by a massive but slow stellar wind. The observed mass loss rates can increase at the late stages of the AGB star up to $\dot{M} \simeq 10^{-4}\,\mathrm{M_\odot\,yr^{-1}}$ (e.g. see review by Habing 1996). In order to get a White Dwarf (WD) with a typical mass of $0.6\,\mathrm{M_\odot}$ from main sequence (MS) masses between 1 and $8\,\mathrm{M_\odot}$ the mass loss must strongly influence the late stellar evolution. Pulsations together with the formation of dust particles provide an effective mechanism to generate such a significant mass loss where the radiation pressure acting on the newly formed dust grains is the main driving force.

Based on these dust formation processes in a carbon-rich environment Dorfi & Höfner (1996) have calculated stationary stellar outflows including the effects of slow stellar rotation. The mass loss rate depends on the polar angle and can be fitted by

$$\dot{M}(\theta) = \dot{M}_p(1 + \epsilon \sin^n \theta) \qquad (1)$$

where $\dot{M}_\mathrm{p}$ denotes the polar mass loss rate, $\varepsilon = \dot{M}_\mathrm{e}/\dot{M}_\mathrm{p} - 1$ and n defines the shape of the angle-dependent mass loss rate function and $\dot{M}_\mathrm{e}$ is the equatorial mass loss rate. This functional dependence has been assumed by Kahn & West (1985) where ε and n have been treated as free asymmetry parameters.

Send offprint requests to: C. Reimers
Correspondence to: reimers@astro.univie.ac.at

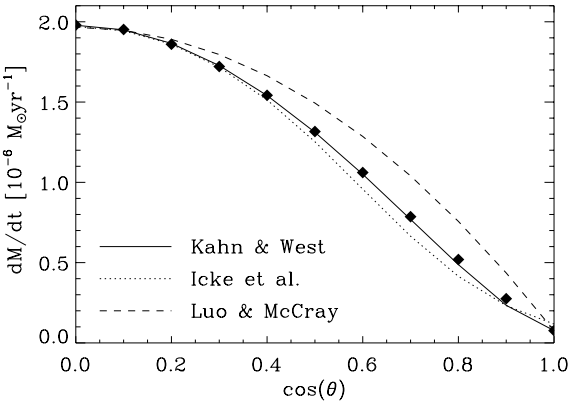

Fig. 1. Different angle-dependent mass loss functions assumed by various authors. The black diamonds represent the mass loss calculations of Dorfi & Höfner (1996) fitted by the solid line (Kahn & West 1985). For comparison we show possible fits by Icke et al. (1989), dotted line, and Luo & McCray (1991), dashed line.

Table 1. Parameters ε and n for four AGB stars with different angular velocities from the calculations of the mass loss rate produced by dust-driven winds (Dorfi & Höfner 1996).

model	ω $[10^{-8}\mathrm{s}^{-1}]$	$v \sin i$ [km/s]	n	ε	$\dot{M}_\mathrm{p}$ $[10^{-6}\,\mathrm{M}_\odot/\mathrm{yr}]$
A	0.5	1.7	2.0	0.3	0.31
B	1.0	3.8	2.1	1.8	0.44
C	1.5	5.1	2.6	7.2	0.74
D	2.0	7.1	3.0	15.1	1.38

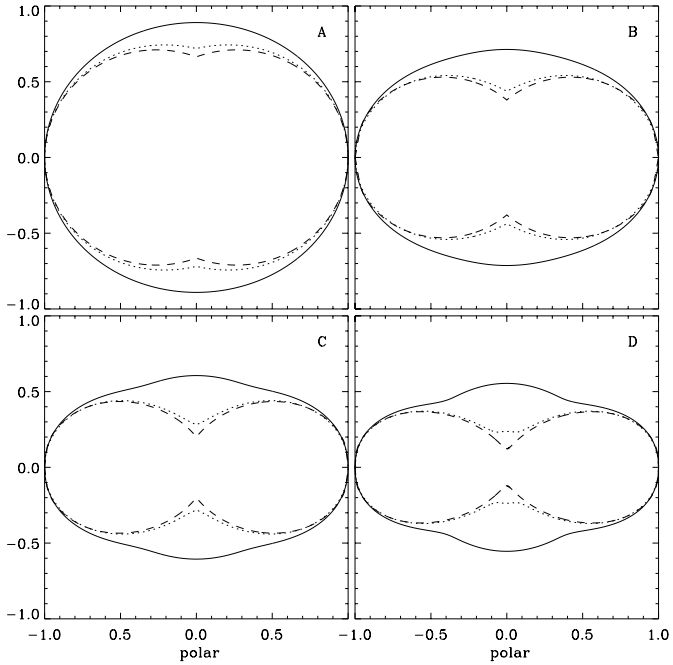

Fig. 2. Shapes resulting from the Interacting Winds Model for the models A, B, C and D in Table 1 and for different values of λ ($\lambda = 2, 5$ and 10 for the the solid, dotted and dashed lines, respectively). For small λ values the results show an elliptical shape. For larger values of λ the shapes are more bipolar. This bipolar structure is more marked in the models C and D with larger values of n (or ε). When the strong-shock approximation breaks down a bulge in the equatorial plane develops in the numerical solution.

Different mass loss dependencies have been assumed e.g. by Icke et al. (1989) and Luo & McCray (1991). Their functional representations are plotted in Fig. 1 for our case D. All curves give reasonable fits within the polar and equatorial regions and more or less small deviations are found at intermediate angles. Since Kahn & West's mass loss dependence (cf. Eq. 1) fits our dust-driven AGB wind model best, we will focus the following discussion on their IWM mass loss formula.

We investigated four models (A to D) in which the AGB stars have different angular velocities. The results for these parameters ε and n together with the resulting mass loss function are summarized in Table 1. The typical outflow velocities of the AGB winds are in the range $V \simeq 5 \ldots 20\,\mathrm{km\,s^{-1}}$ depending on the rotational rate and the polar angle θ, as seen in the result of a non-spherical dust driven wind by Dorfi & Höfner (1996). The maximum degree of condensation and the resulting outflow velocity occur at the equator and decrease towards the rotation axis which reflects the angle dependent mass loss rate function mentioned above.

2.2. Shapes of elliptical PNe

Kahn & West (1985) assumed the angle-dependent mass loss rate function equal to Eq. 1 with the free parameters ε and n as input variables of the IWM. In contrast to their investigation we determine ε and n from the dust driven wind models of AGB stars as a function of the stellar parameters and the rotation rate. A further input parameter, namely

$$\lambda = \frac{U}{V} \tag{2}$$

the ratio of the expansion velocity U of the PN shell to the AGB wind speed V still remains to be specified in the IWM. Assuming a hot shocked gas inside the wind bubble, the flow problem admits a similarity solution in which the radius of the PN shell is proportional to time. For the wind boundary the relation

$$r(\theta, t) = UtF(\theta) \tag{3}$$

holds where $F(\theta)$ defines the so-called shape function depending only on the polar angle θ. To derive a solution for F we require a closed system of equations comprising the conservation equations. This system can be derived by analysing the conservation of mass, the so-called pseudo-angular momentum as well as the pressure balance across the shell boundary (see Kahn & West 1985 for details). Using such a semi-analytic model the form function F can be obtained by a standard integration method. The resulting shapes of $F(\theta)$ are plotted in Fig. 2 in polar coordinates for models A, B, C and D (cf. Table 1) and for different values of λ. Because typical expansion velocities of PNe are $U \simeq 20 \ldots 50\,\mathrm{km\,s^{-1}}$ and AGB wind speeds are up to $V \simeq 20\,\mathrm{km\,s^{-1}}$ the typical λ values can be in the range $\lambda \simeq 1 \ldots 3$.

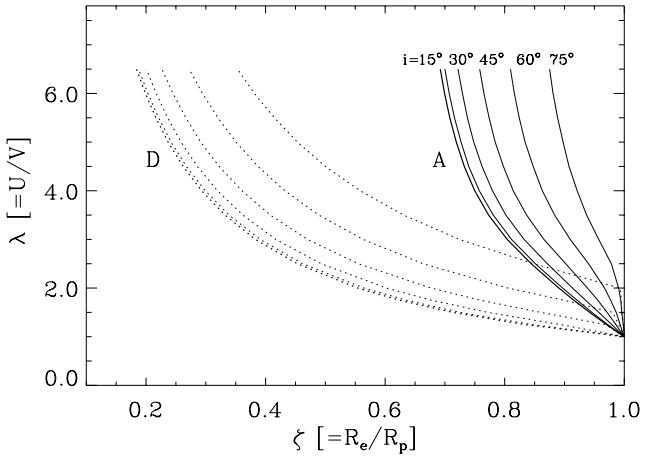

Fig. 3. In this velocity vs. aspect ratio, (λ, ζ)–diagram the ratio (λ) of the expansion velocity of the Planetary Nebula shell U to the AGB wind speed V is plotted against the resulting ratio of the equatorial to the pole aspect of the Planetary Nebula (ζ). The diagram shows the theoretical models A and D (cf. Table 1)with the corresponding curves of the model with increasing inclination i. Taking the different rotation angles of the PNe in the sky into consideration the whole upper right section can be covered with the theoretical shapes.

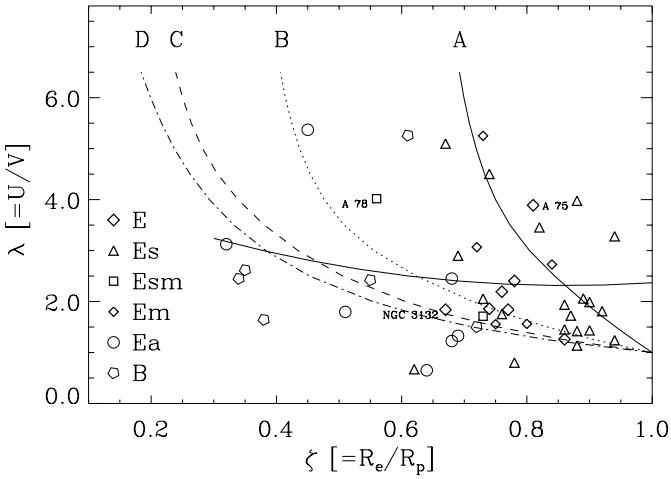

Fig. 4. The same (λ, ζ)–diagram as shown in Fig. 3 with the theoretical models A, B, C and D and 34 observed planetary nebulae listed in Table 2 and the additional object NGC 3132. The value of the AGB wind velocity V is fixed by $12\,\mathrm{km\,s^{-1}}$ and due to a lack of accurate three-dimensional data the inclination is assumed to be $\mathrm{i} = 0$. Further Planetary Nebulae of the types *Ea* (elliptical with ansae) and *B* (bipolar) cannot be described in a satisfactory way by the theoretical model (lower left and lower area). The two planetary nebula of the type *Es* are also not in a state where the models are applicable because they are old and expanded objects so the expansion velocity U will be very low.

2.3. Influence of inclination

Fig. 3 shows a velocity vs. aspect ratio, a (λ, ζ)–diagram in which the lines represent the theoretical models A and D. Also plotted for the models A and D are the lines produced by the different orientations in the sky. The shape of PNe becomes more and more rounder with increasing inclination i. The rotation to an angle of $\mathrm{i} = 75°$ is bound to a relative small area in the (λ, ζ)–diagram. So statistical all PNe which corresponds to models A, B, C or D are in narrow areas right of the respective model line for an angle $\mathrm{i} = 0°$. Since for many PNe the spatial orientation of the shells in the sky is still unknown we will assume in the following sections an inclination of $\mathrm{i} = 0°$.

3. Comparison with observed PNe

3.1. General properties

The theoretical models can only be directly compared to PNe with well-determined parameters, i.e. the spatial dimension and the expansion velocity in the line of sight. For a large number of PNe the dimensions, namely the large and small semi-axes, are given in the *IAC*[1] *Morphological Catalog of Northern Galactic Planetary Nebulae* by Manchado et.al (1996). Based on their data the quantity

$$\zeta(i) = \frac{R_e}{R_p} \tag{4}$$

denoting the ratio of the equatorial to the polar dimension can be specified. Clearly, ζ depends on the sky orientation of the non-spherical shapes.

Furthermore, for many PNe the expansion velocity of the shell is known (e.g. Sabbadin 1984, Weinberger 1989 and the CDS[2]-database). Since we cannot observe the wind speed of the previous AGB star the parameter λ is only poorly quantified by observations for an individual PN. So we fix the wind velocity by $12\,\mathrm{km\,s^{-1}}$ which is the mean value of the dust driven wind models of Dorfi & Höfner (1996). Such PNe of the Table 2 with well known parameters are plotted in Fig. 4.

3.2. Selected PNe

A 75, A 78 – These two PNe are situated above the dividing line (see Sect. 4.2) in the (λ, ζ)–diagram showing cusps which are probably density enhancements produced by an efficent mass loss in the equatoral plane of the previous AGB star. The fast wind from the central object has to react to this distribution of matter. The theoretical calculations can also reproduce this behaviour in the equatorial planes of the PNe (cf. Fig. 5).

NGC 3132 – With a well known orientation (see Sahu & Desai 1986) and an expansion velocity of $v_b = 14.7\,\mathrm{km\,s^{-1}}$ we can derive the point (1.84, 0.67) in the (λ, ζ)–diagram. Now we calculated a model C shape and compared it with an Space Telescope Science Institute (STScI) image from the Hubble Space Telescope (HST). This result is shown in Fig. 6 and we can see that the theoretical shape fits very well with the inner boundary of the PN.

[1] Instituto de Astrofisica de Canarias

[2] Centre de Données astronomiques de Strasbourg

Table 2. Data of 33 observed elliptical Planetary Nebulae from the *IAC Morphological Catalog of Northern Galactic Planetary Nebulae* Classification of the shape, Hα size and expansion velocities $v_{\rm O\,III}$ from the CDS database. Also given are the calculated ζ and λ values for an AGB wind velocity $V = 12\,{\rm km\,s^{-1}}$ and an inclination $\rm i = 0$. Classification of shapes: *E* for Elliptical Planetary Nebula; a suffix s denotes PNe showing an internal structure and m PNe with one or more additional fainter outer shells.

PN G	object	shape	Hα size ["]	ζ	$v_{\rm O\,III}$ [km s^{-1}]	λ
038.1-25.4	A 70	E	48×39	0.81	37.8	3.89
053.3+24.0	Vy 1-2	E	3.8×2.8	0.74	16.5	1.86
094.0+27.4	K 1-16	E	90×70	0.78	22.5	2.40
071.6-02.3	M 3-35	E	5.3×4.1	0.77	17.0	1.84
138.1+04.1	HDW 2	E	373×321	0.86	13.0	1.26
204.0-08.5	A 13	E	146×111	0.76	20.0	2.19
031.0-10.8	M 3-34	Es	10.0×9.4	0.94	14.0	1.24
093.3-00.9	K 3-82	Es	24×22	0.92	20.0	1.81
095.1-02.0	M 2-49	Es	4.2×3.7	0.88	12.0	1.81
095.2+07.8	A 73	Es	85×73	0.86	20.0	1.94
097.5+03.1	A 77	Es	86×67	0.78	7.5	0.80
097.6-02.4	M 2-50	Es	8.9×6.1	0.69	24.0	2.90
101.8+08.7	A 75	Es	60×53	0.88	42.0	3.98
102.8-05.0	A 80	Es	164×120	0.73	18.0	2.05
104.2-29.6	Jn 1	Es	470×405	0.86	15.0	1.45
111.0+11.6	DeHt 5	Es	650×400	0.62	5.0	0.67
112.9-10.2	A 84	Es	148×112	0.76	16.0	1.75
119.6-06.7	Hu 1-1	Es	12.4×11.2	0.90	15.5	1.44
122.1-04.9	A 2	Es	30.0×36.5	0.82	34.0	3.46
128.0-04.1	Simeiz 22	Es	720×530	0.74	40.0	4.50
133.1-08.6	M 1-2	Es	390×340	0.87	18.0	1.72
144.5+06.5	NGC 1501	Es	64×60	0.94	37.0	3.28
159.0-15.1	IC 351	Es	17×15	0.88	15.0	1.42
161.2-14.8	IC 2003	Es	21×19	0.90	21.5	1.99
164.8+31.1	JnEr 1	Es	410×365	0.89	22.0	2.06
205.1+14.2	A 21	Es	765×510	0.67	41.0	5.10
060.8-03.6	NGC 6853	Esm	480×350	0.73	15.0	1.71
081.2-14.9	A 78	Esm	90×50	0.56	27.0	4.02
063.1+13.9	NGC 6720	Em	88×63	0.72	26.5	3.07
064.6+48.2	NGC 6058	Em	32×27	0.84	27.5	2.73
118.0-08.6	Vy 1-1	Em	1.5×1.1	0.73	46.0	5.25
126.3+02.9	K 3-90	Em	7.9×6.3	0.80	15.0	1.56
147.8+04.1	M 2-2	Em	5.3×4.0	0.75	14.0	1.56

4. Discussion

4.1. The theoretical model

Despite the simplicity of the investigated model we find that basically all elliptical PNe with well determined parameters can be interpreted in the framework of IWM based on this angular dependence of the mass loss rate of AGB stars.

The input parameter λ of the IWM, namely the ratio of the expansion velocity of the PN to the AGB wind speed, remains an unknown quantity which is only poorly quantified by observations because we do not know the wind speed of the previous AGB star. In some cases, likely the Helix nebula (NGC 7293), the slow wind speed can be indirectly determined by the motion of the cometary knots in the envelope of the nebula (see e.g. Meaburn et al. 1998). The IWM assumes the AGB wind speed to be independent of the polar angle θ which is not supported by the models for dust-driven outflows. However, since the observations can be reproduced by small rotation rates (cases A and B, see Fig. 4) this assumption of an angle-independent outflow velocity seems not to be a severe restriction to the applicability of the IWM.

4.2. Comparison with observed objects

The development of cusps in the equatorial region can be reproduced if they are interpreted as density enhancements seen in the observations. The dividing line (solid "horizontal" line in Fig. 4) separates the elliptical shapes from the more bipolar ones. Some PNe above this line show such cusps.

In the case of the PNe A 78 (cf. Fig. 5) and NGC 3132 (cf. Fig. 6) we can see how the simple theoretical model fits with images of the nebulae. The nebula A 78 for example shows

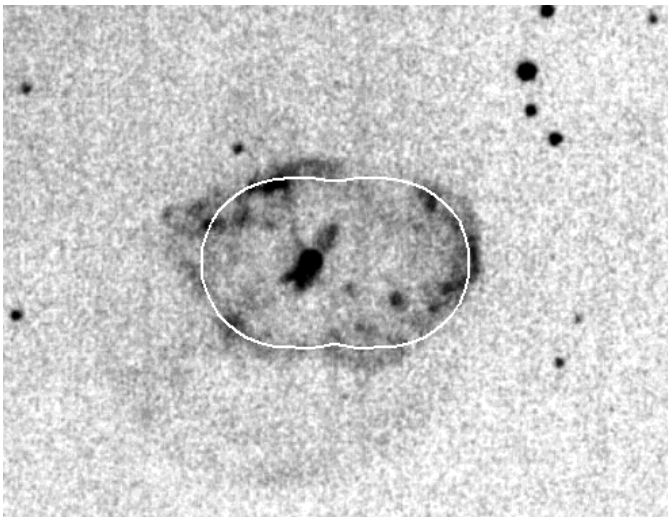

Fig. 5. The planetary nebula A 78 with the fitted model. The theoretical shape shows cusps which are seen as density enhancements in the image of the nebula. [O III] image from the *IAC Morphological Catalog of Northern Galactic Planetary Nebulae* by Manchado et al. (1996).

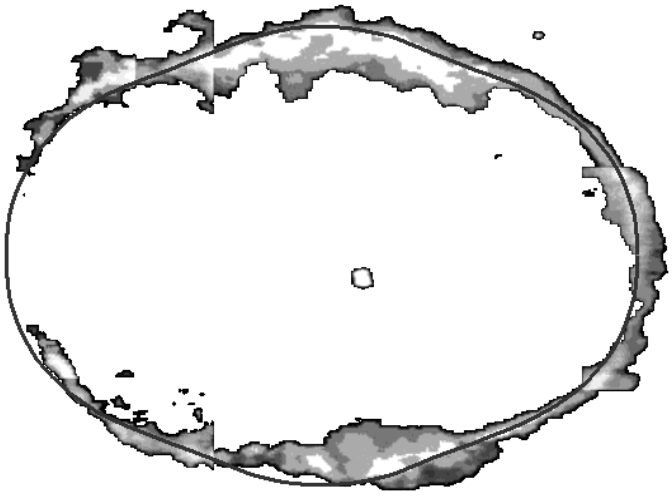

Fig. 6. The planetary nebula NGC 3132 with the fitted model. The bulge-like structure in the image of the nebula also exists in the theoretical shape. The darker edge left and right of the observed planetary nebula shell is artificially brightened for a better comparison of the inner interacting wind boundary with the calculated shape. HST Image STScI-PRC98-39 from the Hubble Heritage Team (STScI/AURA/NASA).

a clumpy but anyhow approximately symmetrical shape with cusps in the equatorial plane. Because of the thickness of the visible wind boundary it is not easy to overlay the calculated shape.

Another problem are selection effects of the observed objects for the morphological classification, e.g. an elliptical or in the worst case a bipolar PN seen from the polar direction ($i = 90°$) is classified in the observed shape as a round PN. Hence, the knowledge of the three-dimensional structure and the orientation in the sky (inclination i) is needed for further investigations of the shaping of PN. To determine the density distribution around the AGB star produced by the mass loss it is important to know what kind of central object powers the PN (e.g. binary, born again object (e.g. Iben 1984), white dwarf). A binary star system can produce a preferential mass loss in the orbital plane (Eq. equatorial plane) forming a more bipolar PN. In some studies of the central objects of bipolar PN (e.g. Corradi & Schwarz 1995, Zhang & Kwok 1998) these stars show a higher average mass than stars in other PN shape types.

4.3. Further effects influencing the shapes

The angle-dependent mass loss in single AGB stars can be explained by a fast rotation. Also a binary star or a planetary system in the center of the PN (see e.g. Corradi & Schwarz 1993 or the HST image STScI PRC99-32) can strongly influence the angle dependency of the mass loss. Massive stars which evolve to so-called "born again" stars produce a multiple shell structure also seen in a lot of PNe. These mainly elliptical shells do not have the same alignment.

Also the location in the galaxy influences the shaping of PNe as explained in Corradi and Schwarz (1995). Because the galactic distribution e.g. of bipolar PNe is comparable to that of main sequence stars (MS) with higher masses while the distribution of elliptical PNe indicates lower progenitor masses (dG stars).

During the late stages of the PN the expanding shell interacts with the ISM. The shape of the PN may become irregular and may also be modified by an interstellar magnetic field (e.g. Soker & Dgani 1997 and Soker & Zucker 1997). In such a case the matter of the PN shell will be locked to the ISM and the central object may decouple from the expanding envelope and leave the geometrical center of the PN as seen in a few objects (runaway central star, e.g. Kerber 1998). Another mechanism to generate an off-center central object is the interaction with a binary star (e.g. in bipolar PNe like MyCn 18).

When the fast but low density wind blows into the dense compressed material Kelvin-Helmholtz and Rayleigh-Taylor instabilities develope (see e.g. Garcia-Segura et al. 1999) resulting in a clumpy boundary. Such changes will first occur in the equatorial plane, where the highest density contrast is present between the dense shell matter and the hot wind bubble.

4.4. Detailed morphology studies

A recent HST analysis like the measurements of the expansion of the PN NGC 6543 (Reed et al. 1999) allows a very accurate study of the evolution of this type of nebula. In the detailed morphology exploration a lot of different shapes have been investigated and features have been observed with different chemical compositions and ionisation levels. Fast outflows, condensations, so-called FLIERS (fast low-ionization emission regions) as well as jet-like phenomena are seen in the outer regions of the nebulae. They can be explained by later high-velocity outbursts based on detailed measurements of spatial proper motion of these features.

The overall structure of a PN is normally not simple. Lobes and filaments are found in young PNe as well as in the surroundings of older PNe. These remnants are probably produced by the dying star during the latest AGB phase ejecting matter by a super wind. Other observed features are distorted ellipsoids and bubbles not interacting with each other. For such investigations it is necessary to consider possible projection effects. For a lot of observed PNe a model with a toroidal or cylindrical structure in the equatorial plane provides the best agreement with the reality. These structures in the equatorial plane can be the result of the massive mass loss in the late stages of the AGB star. The fast wind from the hot central star of the PN can easily escape in the polar directions but not in the equatorial region because of the large amount of matter.

In the outer part of PNe where the matter is less dense and where now no interaction happens a supposed magnetic field can influence the motion of the gas. The central star ionizes the surrounding material and the galactic magnetic field forms structures in the outer part of the PN like stripes seen e.g. in the nebula NGC 6894 discussed by Soker & Zucker (1997).

Also a stellar magnetic field from the post-AGB star can form different shapes of the PN (see e.g. Pascoli 1997 and Garcia-Segura et al. 1999). Therein a compressed magnetic field dominates the motion of the gas and as a consequence the material creates a pair of collimated outflows at the pole and forms a bipolar PN shape.

Other peculiar shapes are the result of hydrodynamical effects like the distinct nose at the end of the lobe of the PN KjPn 8 which can be produced e.g. by environmental gas swept-up by shocks driven by an episodic, collimated, bipolar outflow, the so-called "free stagnation knot" mechanism investigated by Steffen and Lopez (1995).

Some structures can be probably produced by stellar convection cells or cool spots like nonsymmetrical or cometary structures (described e.g. in Soker 1998, Soker & Clayton 1999) due to non-uniform dust formation in the AGB atmosphere which produces knots of denser material blowing away from the fast central object wind.

Acknowledgements. We are grateful to M. Kittel and A. Fritz who gave helpful comments for improving this paper. This work is supported by the *Fonds zur Förderung der wissenschaftlichen Forschung (FWF)* under project number S7305–AST.

References

Iben I., 1984, ApJ 277, 333
Barnbaum C., Morris M., Kahane C., 1995, ApJ 450, 862
Centre de Données astronomiques de Strasbourg (CDS), Planetary Nebulae Catalogue. http://cdsweb.u-strasbg.fr/cgi-bin/myqcat4?VII/24
Corradi R.L.M., Schwarz H.E., 1993, A&A 268, 714
Corradi R.L.M., Schwarz H.E., 1995, A&A 293, 871
Dorfi E.A., Höfner S., 1996, A&A 313, 605
Garcia-Segura G., Langer N., Rozyczka M., Franco J., 1999, ApJ 517, 767
Habing H.J., 1996, A&AR 7, 97
Icke V., Preston H.L., Balick B., 1989, AJ 97, 462
Kahn F.D., 1982. In: Flower XX, Reidel D.R. (eds.) Planetary Nebulae. IAU Symp. No. 130, Reidel, Dordrecht, p. 305
Kahn F.D., West K.A., 1985, MNRAS 212, 837
Kerber F., 1998, Reviews in Modern Astronomy 11, 161
Kwok S., 1982, ApJ 258, 280
Luo D., McCray R., 1991, ApJ 379, 659
Manchado A., Guerrero M.A., Stanghellini L., et al., 1996, The IAC Morphological Catalog of Northern Galactic Planetary Nebulae. Instituto de Astrofisica de Canarias (IAC)
Meaburn J., Clayton C.A., Bryce M., et al., 1998, MNRAS 294, 201
Pascoli G., 1997, ApJ 489, 946
Reed D.S., Balick B., Hajian A.R., et al., 1999, AJ, in press
Sabbadin F., 1984, A&AS 58, 273
Sahu K.C., Desai J.N., 1986, A&A 161, 357
Soker N., 1998, MNRAS 299, 1242
Soker N., Clayton G.C., 1999, MNRAS 307, 993
Soker N., Dgani R., 1997, ApJ 484, 277
Soker N., Zucker D.B., 1997, MNRAS 289, 665
Steffen W., Lopez J.A., 1998, ApJ 508, 696
Weinberger R., 1989, A&AS 78, 301
Zhang C.Y., Kwok S., 1998, ApJS 117, 341